Continuous-Wave Pumping of Multiexciton Bands in the Photoluminescence Spectrum of a Single CdTe-CdSe Core-Shell Colloidal Quantum Dot

Ruth Osovsky,[1] Dima Cheskis,[1] Viki Kloper,[1] Aldona Sashchiuk,[1] Martin Kroner,[2] and Efrat Lifshitz[1,*]

[1]*Schulich Faculty of Chemistry, Russell Berrie Nanotechnology Institute, Technion, Haifa 32000, Israel*

[2]*Institute of Quantum Electronics, ETH Zurich, CH-8093 Zurich, Switzerland*

(Received 19 July 2008; published 14 May 2009)

Single-exciton, biexciton, triexciton, and quadraexciton bands were resolved in the microphotoluminescence spectrum of a single CdTe/CdSe core-shell colloidal quantum dot, revealing nearly blinking-free behavior. Multiexcitons were generated by a sequential filling of electronic shells with the increase of a continuous-wave excitation power, and their probability was evaluated under steady-state conditions. A partial carriers' delocalization was determined at the core-shell interface, and an exciton binding energy was estimated by a second-order perturbation theory.

DOI: 10.1103/PhysRevLett.102.197401 PACS numbers: 78.67.Hc, 78.55.Et, 78.67.Bf

Radiative recombination of multiexcitons in semiconductor quantum dots is a topic of a special scientific and technological interest. These radiative processes were thoroughly investigated in self-assembled quantum dots [1,2], revealing the strong influence of many-body Coulomb and exchange interactions on the electronic properties of quantum confined systems [3]. However, radiative processes of this kind were belatedly found in colloidal quantum dots (CQDs) capped with organic ligands [4–6]. Multiexcitons in CQDs are ''squeezed'' into a single-exciton volume, and they experience low dielectric screening by the organic surfactants, and thus, they decay primarily via nonradiative Auger relaxation at a time scale of 10–100 ps [7,8]. Furthermore, Auger relaxation creates luminescence blinking in a single CQD detection with ''on'' and ''off'' power law time distribution, while this process was shown to be partially reduced in the detection of the luminescence of a single colloidal nanorod [6,8]. Theoretical predictions of the energetic and lifetime of multiexcitons in CQDs were given in Refs. [9,10]. On the practical side, the fast nonradiative Auger recombination restricts the time during which photoexcited multiexcitons can be extracted from CQDs in photovoltaic cells [11] or maintain an inversion of population in gain devices [12], while the blinking limits the CQDs' application as biological labels [13]. Thus, defeat of an Auger process and the ease of detection of radiative multiexciton recombination in CQDs is a timely topic.

In this Letter, we report for the first time well-resolved neutral single-exciton (X), biexciton (BX), triexciton (TX), and plausible quadraexciton (QX) emission bands in the microphotoluminescence (μ-PL) spectrum of a *single* CdTe/CdSe core-shell CQD, pumped by a continuous-wave (cw) excitation and exhibiting nearly blinking-free behavior. The multiexcitons were generated by a sequential filling of the s and p shells with an increase of excitation power, when recorded at 4.2 K. The investigated core-shell structures offered a few advantages with respect to simple CdTe cores: (a) an increase of the effective CQD's volume, (b) improved surface quality, and (c) a reduction of the dielectric contrast between the core and its immediate surrounding. In some ways, the core-shell CQDs mimic self-assembled quantum dots embedded in a semiconductor matrix. The structures also allow controlling the carriers' spatial distribution between the core and the shell by varying the ratio between the core radius and the shell thickness [14]. The observation of multiexcitons' emission under cw pumping is direct evidence for a partial or a complete suppression of an Auger process in the studied core-shell CQDs.

The synthesis of CdTe/CdSe core-shell CQDs was based on a similar procedure given in Ref. [14]. Representative absorption (solid lines) and the emission (dashed lines) spectra of CdTe cores, with an average radius of $R = 1.6$ nm, and the corresponding CdTe/CdSe core-shell CQDs, with shell thickness of Th = 0.6 nm, are shown in Fig. 1. The core-shell CQDs exhibit exceptionally high emission quantum efficiency (QE) of 88%. A transmission electron microscope (TEM) image of the CdTe/CdSe CQDs is shown in the left inset. A Fourier transform of this image, as well as an x-ray diffraction measurement (not shown), revealed the existence of a zinc-blende CdTe lattice (space group $F\bar{4}3m$) over the entire core-shell structure. The right inset in the figure illustrates a hole (blue curve) and an electron (red curve) radial density distribution $[r^2\rho(r)^2]$ over the entire core-shell structure, revealing a slight delocalization of the electron into the shell region, approaching a quasitype II configuration. The density distribution was evaluated by an effective-mass approximation theory [15], assuming continuity of the wave functions and effective-mass-weighted derivatives at the heterointerface, considering the dielectric constant $\varepsilon_\infty(\mathrm{CdTe}) = 7.2$ and $\varepsilon_\infty(\mathrm{CdSe}) = 5.6$, and a bulk valence and conduction band offsets of 0.5 eV and 0.3 eV, respectively [16].

The μ-PL spectra of a single CdTe and CdTe/CdSe CQDs, dispersed over a quartz substrate with a density

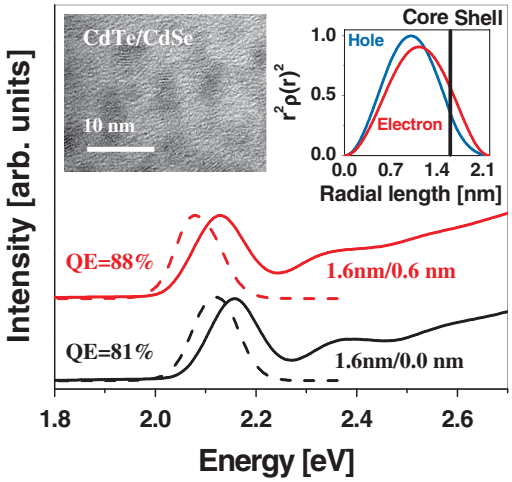

FIG. 1 (color). Absorption (solid lines) and the emission (dashed lines) spectra of CdTe core CQDs with $R = 1.6$ nm (bottom curves) and the corresponding CdTe/CdSe core-shell CQDs (top curves) with a shell thickness of Th = 0.6 nm. Insets: A TEM image (left) and a radial density distribution $[r^2\rho(r)^2]$ of a hole (blue curve) and an electron (red curve) of the core-shell CQDs.

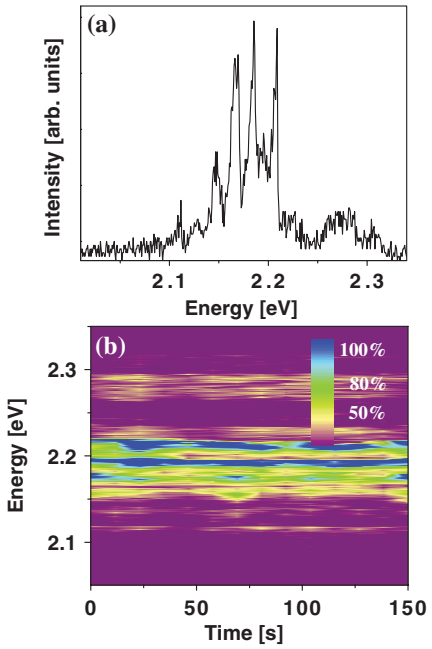

FIG. 2 (color). (a) Representative μ-PL spectrum of a single CdTe/CdSe CQD, recorded at 4.2 K, illuminated by a cw laser with excitation energy of 2.41 eV and a power of $P = 30$ μW. (b) A contour plot of the μ-PL intensity (see side ruler) versus the emission energy and the accumulation time. The minor intensity variations reflect a suppression of an Auger process.

<1 CQD/μm^2, were recorded by the use of a fiber-based confocal microscope (Attocube attoCFM I), immersed in a cryogenic system, similar to the setup described in Ref. [17]. The samples were pumped by a cw-Ar^+ laser ($E_{exc} = 2.41$ eV) with a power, P, varying from 10 to 100 μW, a diffraction limited full width at half maximum spot of ~ 1 μm^2. A μ-PL spectrum of a single CdTe/CdSe CQD, recorded at $P = 30$ μW and integrated over 10 s, is presented in Fig. 2(a). This spectrum consists of several intense zero-phonon bands (with a resolution that is limited by the instrument resolution to ~ 1 meV), accompanied by some satellites and a weak broad pedestal, which appears only under high illumination intensity. The multiband nature of the μ-PL spectrum was reproducible in various single core-shell CQDs; each showed a unique spectral stability, enabling the recording of successive spectral frames over a period of 1 to 2 days. This is in contrast to the nature of a single CdTe core, which deteriorated after a trace of a single μ-PL frame, and showed only a single band spectrum (not shown). The bands presented in Fig. 2(a) are unevenly spaced ($\Delta E \sim$ 19–24 meV) and attenuated differently with the variation of the excitation power (*vide infra*). This evidence excludes the existence of optical-phonon replica [18], and instead suggests the occurrence of multiexcitons recombination. Figure 2(b) shows a contour plot of the μ-PL bands' intensity versus the emission energy and the time evolution. This plot encompasses important characteristics; the intensity of the higher energy bands undergoes only minor intensity fluctuations $<10\%$ and a small spectral diffusion, revealing a nearly blinking-free behavior.

Figure 3 demonstrates the evolution of the μ-PL of a single CdTe/CdSe CQD, with the increase of laser power, P, when $P_0 = 10$ μW. The red and green bands show an increase of the emission intensity up to $\sim 3.5P_0$ and $6.5P_0$, respectively, but they fade away above those power levels. These bands are also accompanied by satellites that are still visible at the highest pumping power applied. The satellites, shifted away from the dominant bands by ~ 3 meV, may be related to a minor appearance of charged excitons (e.g., X^+, $2X^+$) or the appearance of acoustic phonon replica [19]. The charged exciton has a low probability due to the absence of a charge injection from a wetting layer or hydrophobic ligands, as well as a low Auger ionization in nearly blinking-free CQDs. The spectra recorded at $6.5P_0$ show additional broad bands (colored blue and yellow), emerging simultaneously on the high and low energy sides of the spectra. Plots of the strength of the μ-PL bands between 2.13 and 2.23 eV versus the laser power are shown by the symbols in Fig. 4(a) (the solid lines guide the eye). The general trends of these plots were compared with a theoretical estimation of the probability of finding the Nth neutral multiexciton (n_N), under a certain P, using the following analytical equation:

$$n_N(P) = n_0(P)P^N \prod_j^N \tau_j,$$
$$n_0(P) = \frac{1}{1 + \tau_1 P + \tau_1\tau_2 P^2 + \ldots P^N \prod_j^N \tau_j}. \quad (1)$$

This expression was derived from a general kinetic consideration (Ref. [1]), assuming a time-independent

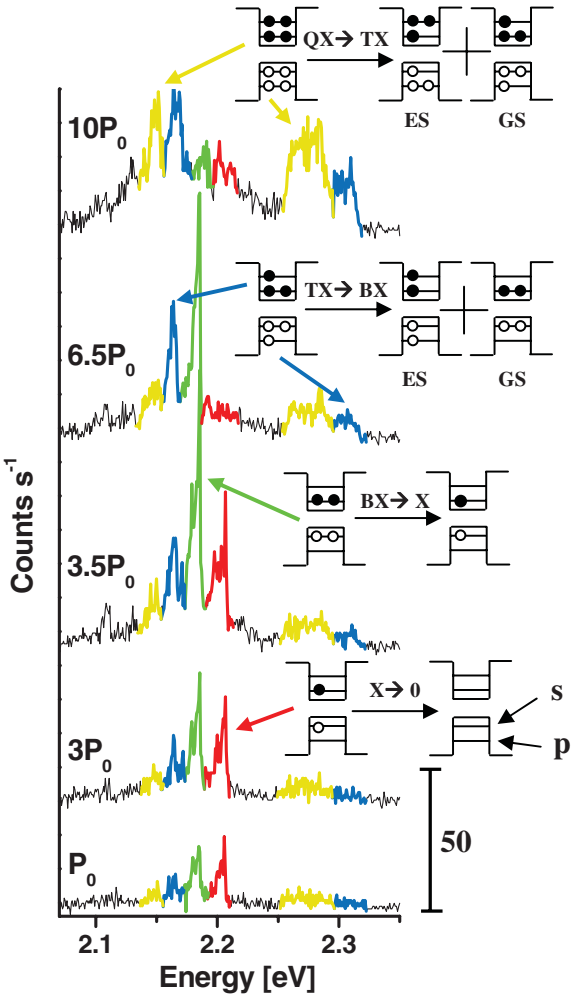

FIG. 3 (color). A sequence of μ-PL spectra of a single CdTe/CdSe core-shell CQD, excited with a variable laser power (when $P_0 = 10\ \mu$W) and recorded at 4.2 K. The possible electron-hole annihilation processes from the s and p shells are drawn schematically in the inset diagrams.

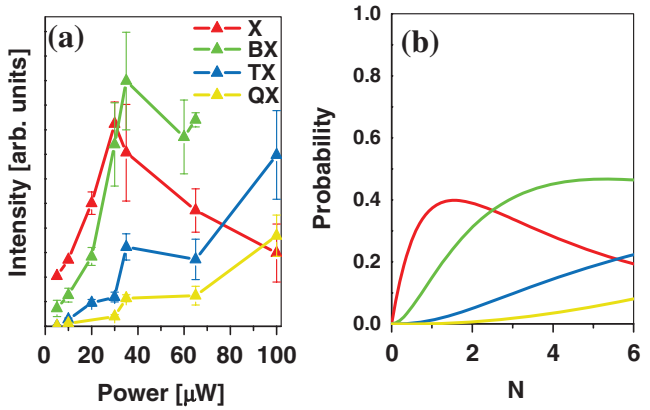

FIG. 4 (color). (a) Dependence of the integrated intensity of a single CdTe/CdSe μ-PL band, between 2.13 and 2.23 eV, versus the excited laser power, P (symbols designate the experiment, while the solid line only guides the eye). (b) Theoretical evolution of the population of neutral single and multiexcitons, versus the numbers of excitons, N.

pumping and a steady-state population ($dn_N/dt = 0$). Equation (1) reveals a unified dependence of the various excitons on P when $0 < n_N < 1$. n_0 is the probability of simultaneous existence of all N excitons generated at a given P. τ_j is the radiative lifetime of the jth multiexciton ($j = 1, 2, 3, \ldots, N$). Although the measured decay time may be different from the radiative lifetime (due to nonradiative effects), we used the value of a measured decay time here, in view of the large emission quantum efficiency of the studied samples. We refer to a measured decay time of a single exciton of an ensemble of CQDs of $\tau_1 \sim 800$ ns at 4.2 K (or $\tau_1 \sim 12$ ns at 300 K) [20]. The evaluation of a multiexciton's lifetime was based on the following points: (a) A multiexciton emits a photon only from its ground state (GS) at 4.2 K. (b) The decay time of the Nth multiexciton is shorter than τ_1 by a factor related to the number of possible transitions into the $(N-1)$th exciton, with a change in the total angular momentum of ± 1, thus, $\tau_2 = 1/2\tau_1$, $\tau_3 = 1/6\tau_1$, and $\tau_4 = 1/4\tau_1$. Finally, plots of occupation probabilities, n_N, versus N are drawn in Fig. 4(b). The similarities between the trends of Fig. 4(a) and 4(b) are pronounced in the nonlinear growth of the green, blue and yellow curves, as well as the saturation and quenching turning points of the curves. It suggests that the red, green, blue and yellow curves correspond to the neutral X, BX, TX and QX recombination emissions, respectively. Accordingly, the electronic configuration of the multiexcitons discussed and the ground-state recombination processes are drawn schematically in the insets of Fig. 3. It should be noted that at any given time, only one type of exciton exists; however, multiexcitons are visible simultaneously in the μ-PL spectra when data accumulation occurs over 10 s.

Additional fingerprints support the occurrence of TX and QX: (A) The TX-GS, labeled in Fig. 3, has a total angular momentum $J = 0, \pm 1$. Electron-hole (e-h) exchange interaction creates a split, inducing an emission from the $J = \pm 1$ at 4.2 K (not shown). The total angular momentum of the BX-GS is $J = 0$, while that of the BX excited state (ES) is $J = 0, \pm 1, \pm 2, \pm 3$ (considering a heavy hole of $J = \pm 3/2$, while all other states possess $J = \pm 1/2$). Obeying the selection rule of $\Delta J = \pm 1$, an allowed e-h annihilation from TX($J = \pm 1$) into BX($J = 0$) via the p-p channel has a twofold degeneracy, appearing in Fig. 3 as a weak blue band at the high energy side of X, with an energy shift slightly smaller than the s-p shell spacing ($\sim$200 meV), due to the existence of many-body Coulomb interactions [3,21]. An allowed transition from TX($J = \pm 1$) into the excited state BX($J = 0, \pm 2$) via the s-s channel has a fourfold degeneracy (twice that of a decay into BX-GS), emerging as an intense blue band at 2.16 eV. (B) The QX-GS has an angular momentum of $J = 0$, undergoing e-h annihilation into TX-GS ($J = \pm 1$) and TX-ES ($J = \pm 1$) via the p-p and the s-s channels, respectively, both with a twofold degeneracy. Thus, QX $\rightarrow$ TX

transitions are depicted as broad bands on both sides of X (yellow bands in Fig. 3) with nearly equal intensities, distinguishable from the TX → BX transitions. (C) A plausible relaxation of $TX^+(J = \pm 1/2)$ could have occurred via the *s-s* route into a $BX^+(J = \pm 1/2, \pm 3/2)$, which would have appeared only on the low energy side of X, in disagreement with the blue and yellow bands appearing in Fig. 3.

The energy shifts (ΔE_i) between adjacent emission bands with peak energy E_i (i = X, BX, TX, QX), are related to the binding energies of the multiexcitons, when $\Delta E_{BX} = 2E_X - E_{BX}$, $\Delta E_{TX} = 3E_X - E_{TX}$ or $\Delta E_{TX} = E_X + E_{BX} - E_{TX}$, and $\Delta E_{QX} = E_X + E_{TX} - E_{QX}$ or $\Delta E_{QX} = 2E_{BX} - E_{QX}$. However, the energy of any *e-h* recombination in the presence of other spectators depends on the existence of attractive and/or repulsive Coulomb interactions. The influence of those interactions is evaluated by a standard second-order perturbation treatment. For example, explicit determination of ΔE_{BX} is based on the eigenenergies of X and BX, as given by the Eqs. (2) and [3].

$$E_i = E_0 + \langle 0|H_i'|0\rangle + \sum_{\alpha} \frac{|\langle 0|H_i'|\alpha\rangle|^2}{E_0 - E_\alpha}, \tag{2}$$

where E_0 and $\langle 0|$ are the unperturbed eigenenergy and eigenvector of the *e-h* ground state based on a kinetic energy, E_α, and $\langle \alpha|$ is an unperturbed eigenenergy and eigenvector of a higher energy state referring to one or more *e-h* pairs, and H_i' is the many-body perturbation operator given in Eq. (3):

$$H_i' \propto \frac{1}{2} \sum_{a,b,=1}^{k} q_a q_b \frac{\varepsilon - 1}{\varepsilon_{CQD} R_{ov}} \sum_{l=0}^{\infty} \left(\frac{\vec{r}_a \vec{r}_b}{R_{ov}^2}\right)^l P_l\left(\frac{\vec{r}_a \vec{r}_b}{r_a r_b}\right) \times \frac{1}{1 + \varepsilon l/(l+1)} \tag{3}$$

when a and b label two particles with a charge q, k is the number of particles, R_{ov} is the overall core-shell radius, r_a and r_b are the positions of two different charges, and P_l is a Legendre polynomial function. $\varepsilon = \varepsilon_{CQD}/\varepsilon_S$ when ε_{CQD} and ε_S correspond to the dielectric constant of the CQD and the surfactant surrounding, respectively. It should be noted that the consideration of the different dielectric constants of the core and the shell components is already buried within the calculations of the overall ground-state eigenvector of quasitype II core-shell CQD, while the surfactant surrounding is included here as a surface polarization effect [21]. In Eqs. (2) and (3), ΔE_{BX} was evaluated as 12 meV. The simplified theoretical model described above, which ignored the contribution of high energy states to the perturbation, enabled supplying only an order of magnitude evaluation to the binding energy. The explicit calculation of the binding energy was rarely done in CQDs, and if so, only by the use of a classical electrostatic model, assuming a complete charge separation between a core and a shell [12], which is not appropriate for our case.

In summary, the utilization of low temperature μ-PL unambiguously indicated the multiexciton photoluminescence in a single quasitype II CdTe/CdSe core-shell CQD, under continuous-wave pumping. The observation of multiexciton recombination is direct evidence for the suppression of the nonradiative Auger recombination in the studied structures. The study is an important contribution to practical use of such CQDs in biological labeling, gain devices, and photovoltaic cells, when multiexciton species or nonblinking effects determine the application functionality. This study presented basic results, the first of their kind, which will be further clarified in the near future by measuring spectral splitting in the presence of an external magnetic field, or concrete distinctions via temporal resolution.

The authors thank Dr. Olga Solomeshch for carrying out the QE measurements and acknowledge support from the Israel Science Foundation (Projects No. 1009/07 and No. 1425/04), the USA-Israel Binational Science Foundation (No. 2006-225), and the Ministry of Science (No. 3-896).

*Corresponding author.
ssefrat@techunix.technion.ac.il

[1] E. Dekel *et al.*, Phys. Rev. B **62**, 11 038 (2000).
[2] M. Ediger *et al.*, Nature Phys. **3**, 774 (2007).
[3] L. Banyai and S. W. Koch, *Semiconductor Quantum Dots* (World Scientific Press, Singapore, 1993).
[4] J. M. Caruge *et al.*, Phys. Rev. B **70**, 085316 (2004).
[5] D. Oron, M. Kazes, and U. Banin, Phys. Rev. B **75**, 035330 (2007), and references within.
[6] N. Le Thomas *et al.*, Appl. Phys. Lett. **89**, 263 115 (2006).
[7] V. I. Klimov *et al.*, Science **287**, 1011 (2000).
[8] Al. L. Efros and M. Rosen, Phys. Rev. Lett. **78**, 1110 (1997).
[9] J. Shumway *et al.*, Phys. Rev. B **63**, 155316 (2001).
[10] A. Franceschetti and M. C. Troparevsky, J. Phys. Chem. C **111**, 6154 (2007).
[11] A. J. Nozik, Physica (Amsterdam) **14E**, 115 (2002).
[12] V. I. Klimov *et al.*, Nature (London) **447**, 441 (2007), and references within.
[13] Al. L. Efros, Nature Mater. **7**, 612 (2008); Y. Chen *et al.*, J. Am. Chem. Soc. **130**, 5026 (2008); B. Mahler *et al.*, Nature Mater. **7**, 659 (2008).
[14] V. Kloper *et al.*, J. Phys. Chem. C **111**, 10 336 (2007).
[15] D. Schoos *et al.*, Phys. Rev. B **49**, 17 072 (1994).
[16] A. H. Nethercot, Phys. Rev. Lett. **33**, 1088 (1974).
[17] R. J. Warburton *et al.*, Nature (London) **405**, 926 (2000).
[18] P. M. Amirtharaj and F. H. Pollak, Appl. Phys. Lett. **45**, 789 (1984).
[19] M. J. Fernée, J. Phys. Chem. C **112**, 1878 (2008).
[20] R. Osovsky *et al.*, J. Phys. Chem. C **111**, 10 841 (2007); D. Dorfs *et al.*, Small **4**, 1148 (2008).
[21] L. Brus, J. Chem. Phys. **80**, 4403 (1984).